

# **Algorithm Theoretical Basis Document (ATBD) for satellite-based Arctic Ocean Primary Productivity assessment**

**Version 1.0**

**Simon Bélanger,  
Université du Québec à Rimouski (UQAR) and Arctus inc**

**And**

**Marcel Babin,  
CNRS and Université Laval**

**March 2011**

## Table of Contents

<b><u>1. INTRODUCTION AND RATIONALE .....</u></b>	<b><u>1</u></b>
<b><u>2. THE APPROACH.....</u></b>	<b><u>2</u></b>
<b><u>2.1 THE ATMOSPHERE-OCEAN LIGHT PROPAGATION MODEL .....</u></b>	<b><u>3</u></b>
2.1.1. DIFFUSE ATTENUATION COEFFICIENT FOR IN-WATER DOWNWELLING IRRADIANCE .....	4
<b><u>2.2. THE PHOTOSYNTHESIS MODEL AND ITS PARAMETERIZATION.....</u></b>	<b><u>5</u></b>
<b><u>2.3 COMPUTATION SPECIFICATIONS .....</u></b>	<b><u>7</u></b>
<b><u>3. MODEL'S INPUTS.....</u></b>	<b><u>9</u></b>
<b><u>3.1. OCEAN COLOR DATA.....</u></b>	<b><u>9</u></b>
<b><u>3.2 ATMOSPHERIC DATA .....</u></b>	<b><u>11</u></b>
<b><u>3.3 SEA ICE DATA .....</u></b>	<b><u>11</u></b>
<b><u>4. SENSITIVITY ANALYSIS.....</u></b>	<b><u>12</u></b>
<b><u>4.1. IMPACT OF OCEAN COLOR DATA AVAILABILITY .....</u></b>	<b><u>13</u></b>
<b><u>4.2. IMPACT OF THE METHOD USED TO CALCULATE THE CLIMATOLOGY .....</u></b>	<b><u>15</u></b>
<b><u>5. KNOWN LIMITATIONS OF THE METHODOLOGY .....</u></b>	<b><u>19</u></b>
<b><u>6. CONCLUSIONS .....</u></b>	<b><u>22</u></b>
<b><u>7. BIBLIOGRAPHY .....</u></b>	<b><u>23</u></b>

## 1. Introduction and rationale

**Primary production** (PP) in the marine environment is defined as the production of organic compounds from sunlight, inorganic nutrients and aquatic carbon dioxide through the process of photosynthesis. Primary production is distinguished as either *net* or *gross* where the former accounts for losses due to processes such as cellular respiration while the latter does not. Satellite ocean-color radiometry is a powerful tool to detect the responses of the marine ecosystem productivity to changes in their physical environment. It provides quantitative assessment of the biological state of the surface ocean at synoptic and temporal scales inaccessible from traditional field observations. Among geophysical products derived from ocean-color data, **chlorophyll-a** (*chl*), the pigment that is responsible for the photosynthesis of organic carbon in the ocean, is the most important when assessing the oceanic primary production.

Several empirical and semi-analytical methods have been proposed in the literature for the estimation of primary production from ocean-color observations. Thorough intercomparisons of existing PP models were conducted by Campbell et al. (2002) and Carr et al. (2006). The best models provide PP estimates that vary within a factor of two from true PP (determined from *in situ* measurements). Unlike empirical models (e.g. Behrenfeld and Falkowski 1997), semi-analytical models can be tuned more easily because they are parameterized with measurable quantities and they allow the accounting for the spectral nature of light, whose variations are known to be significant in coastal waters (e.g. Platt et al. 1988, Sathyendranath et al. 1989, Morel 1991). Indeed, most PP models have been developed for clear open ocean waters known as case-1 waters (e.g. Antoine and Morel, 1996; Behrendfeld and Falkowski 1996; Behrenfeld et al., 2005; Arrigo et al 1998; Pabi et al 2008). They often rely on statistics that are strictly valid for Case 1 waters only. For instance, in the model developed by Morel (1991), the diffuse attenuation coefficient that is used to determine the scalar irradiance at every depth in the euphotic zone, is a function of *chl* only (Morel 1988). Smyth et al (2005) showed that using such a model in coastal waters influenced by chromophoric dissolved organic matter (CDOM) leads to an overestimation of PP. The same authors proposed a method for case-2 waters that accounts for the presence of CDOM.

The Arctic Ocean is characterized by large continental shelves that receive enormous amounts of organic matter-rich river runoff. Despite its small size that is approximately 1% of all oceans, the Arctic Ocean receives about the 10% of the global surface runoff, making these waters optically complex. Current models employed to study the Arctic Productivity (Pabi et al 2008, Arrigo et al 2008; Perrette et al 2010) do not account for the presence of highly absorbing substances such as CDOM or non-algal and mineral particles (NAP). In addition, persistent sea ice and frequent cloud cover in the Arctic was not addressed specifically by most of the

published satellite-based PP models.

The objective of this document is to present the implementation of an semi-analytical PP model that was developed specifically for the Arctic waters. The current document will first describe the overall approach. Each component of the model will then be described in details. To conclude, the limitations of the model will be briefly discussed and perspectives for the future will be given.

## 2. The approach

Our approach makes use of the state-of-the-art development in ocean color (OC) remote sensing. It also combines various satellite observations, namely sea ice and cloud properties in order to model the incident spectral solar irradiance below the sea surface,  $E_d(\lambda, 0)$ . As we deal with optically complex waters, all calculations were made considering the full spectral irradiance. The full-spectral PP model has been implemented in Fortran 90 to quantify photosynthesis in the Arctic Ocean.

The model contains two main components (Figure 1): **1)** a spectral model of light propagation through the atmosphere and the Ocean (Fig. 1; dark blue box) **2)** chl estimations from ocean color OC images and **3)** a model for photosynthesis. The components 1 and 3 will be presented in chapter 2 while the component 2, in chapter 3.

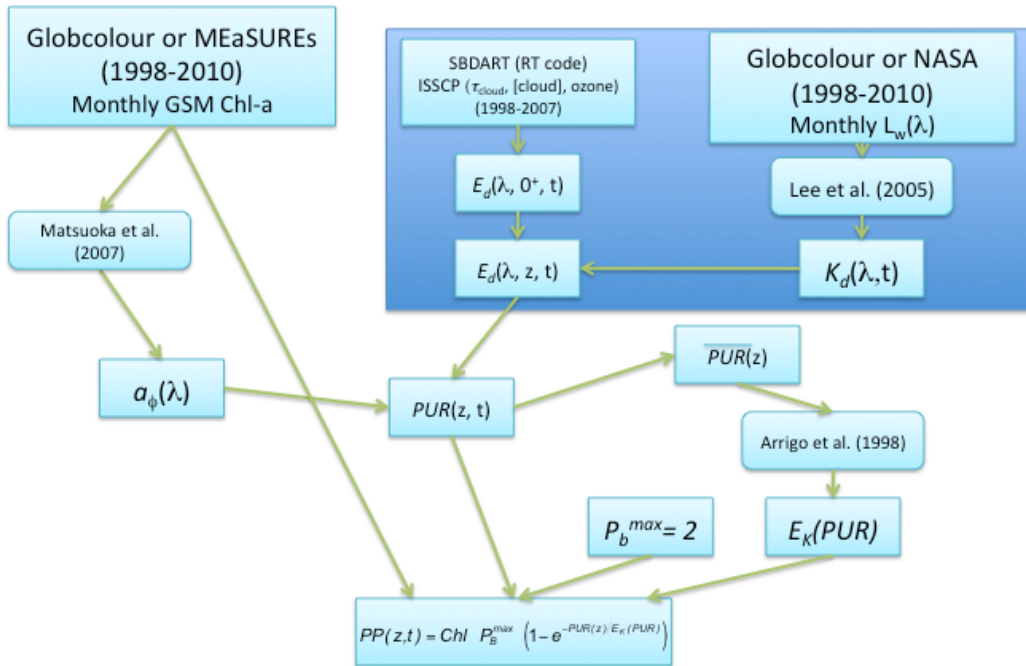


Figure 1 – Flowchart summarizing the structure of the PP model (see text for details).

## 2.1 The atmosphere-ocean light propagation model

Solar radiation reaching the sea surface depends primarily on the sun's elevation and the presence (or absence) of a cloud cover. Atmospheric pressure, aerosols and various atmospheric gases (ozone and water vapor) are also among the factors that control the optical thickness of the atmosphere. Here we make use of an atmospheric radiative transfer model (SBDART) developed by Ricchiazzi et al (1998) to generate look-up-tables of the spectral irradiance just below the sea surface,  $E_d(\lambda, 0^+)$ , in the UV/visible domain (hereafter named EdLUT). The direct and diffuse components of the incident irradiance  $E_{ddir}(\lambda, 0^+$  and  $E_{ddif}(\lambda, 0^+)$  were computed at every 5 nm from 290 to 700 nm using SBDART. Computation were made with:

- 19 different values for sun's zenith angle ( $\theta_s$ ) from  $0^\circ$  to  $90^\circ$  at every  $5^\circ$ ;
- 8 values for total ozone column ( $O_3$ ) from 200 to 550, in Dobson units (DU) at every 50 DU;
- 8 values for could optical thickness ( $\tau_{cl}$ ) from 0 to 64, i.e. 0, 1, 2, 4, 8, 16, 32 and 64;
- marine aerosols with an optical thickness equal to 0.1 at 550 nm;
- a subarctic summer atmosphere (McClatchey et al, 1971), defining standard vertical

profiles of pressure, temperature and water vapor.

Assuming that the specular reflection by the air-sea interface depends on the angular distribution the light field, the underwater irradiance is calculated as follows :

$$E_d(\lambda,0-) = E_{ddif}(\lambda,0+) \times (1 - 0.066) + E_{ddir}(\lambda,0+) \times (1 - \rho_{fresnel}) \quad (1)$$

where  $\rho_{fresnel}$  is the specular reflection coefficient and is calculated as a function of the sun's zenith angle and the refraction indexes of air and water. Note that our assumption of a flat water surface may tend to overestimate the specular reflection at very low solar elevations. EdLUT is, hence, a four-dimensional LUT with a total of 100928 elements. It requires as input  $\lambda$ ,  $\theta_s$ ,  $O_3$  and  $\tau_{cl}$ . To calculate the irradiance for a given ocean pixel, the fraction of the sky occupied by the cloud (CF) is also needed to be known. When CF is equal to 0,  $\tau_{cl}$  is set to 0 to obtain a clear sky spectrum. When CF is greater than 0, then

$$E_d^{pixel}(\lambda,0-) = E_d^{CLOUD}(\lambda,0-) \times CF + E_d^{CLEAR}(\lambda,0-) \times (1 - CF), \quad (2)$$

where  $E_d^{CLOUD}(\lambda,0-)$  and  $E_d^{CLEAR}(\lambda,0-)$  were obtained from the EdLUT with the actual  $\tau_{cl}$  value and  $\tau_{cl} = 0$  respectively. The water column was divided in 12 optical depths ( $z$ ): 100%, 90%... 10%, 1% and 0.1% using the following equation :

$$E_d^{pixel}(\lambda,z) = E_d^{pixel}(\lambda,0-) \exp[-K_d(\lambda) \cdot z], \quad (3)$$

where  $K_d(\lambda)$  is the under-water spectral diffuse attenuation coefficient.

### 2.1.1. Diffuse attenuation coefficient for in-water downwelling irradiance

The diffuse attenuation coefficient for downwelling irradiance,  $K_d(\lambda)$ , is an apparent optical property (AOP) that is tightly related with the inherent optical properties (IOPs) of the seawater constituents, namely the total absorption ( $a$ ) and backscattering ( $b_b$ ) coefficients. IOPs can be assessed from space-borne OC radiometric observations. In the current study, the method proposed by Lee et al 2005a and validated by Lee et al 2005b was adopted. Unlike the empirical approaches that were developed for case 1 waters (e.g. Morel 1988; Morel and Maritorena 2001), the Lee et al.'s model also works in case 2 waters. Briefly, the approach consists of :

- 1) the retrieval of the spectral absorption  $a(\lambda)$  and the backscattering  $b_b(\lambda)$  coefficients from the water-leaving reflectance spectra  $R_{rs}(\lambda)$  using a quasi-analytical algorithm (QAA) (Lee et al., 2002), and
- 2) a semianalytical model for  $K_d(\lambda)$  that is based on the radiative transfer equation (Lee et al., 2005a) and that takes as input  $a(\lambda)$ ,  $b_b(\lambda)$  and the sun's zenith angle ( $\theta_s$ ).

The QAA was implemented in Fortran 90 to retrieve IOPs from the  $R_{rs}(\lambda)$  provided either by the merged imagery products of the ESA Globcolour project (<http://www.globcolour.info/>) or SeaWiFS images from NASA (<http://oceandata.sci.gsfc.nasa.gov/>). To date, only the following SeaWiFS spectral bands were used in the  $R_{rs}$  inversion : 412, 443, 490, 510, 555 and 670 nm.  $K_d(\lambda)$  was calculated using the equation by Lee et al (2005a) :

$$K_d(\lambda, \theta_s) = m_0(\theta_s)a(\lambda) + m_1(\theta_s)(1 - m_2(\theta_s)e^{-m_3(\theta_s)a(\lambda)})b_b(\lambda) \quad (4)$$

where  $m_0$  to  $m_4$  are coefficients for an average  $K_d(\lambda)$  for the euphotic zone which is defined as the upper water layer bound by the surface and the depth of 10% of the incident light (Table 1). This is the layer that contributes most to the photosynthesis of the total water column (Antoine et al., 1995; Platt, 1986).

Table 1 –  $K_d(\lambda)$  model parameters for the euphotic zone for three values for sun's zenith angle

	Sun Zenith Angle		
	10°	30°	60°
$m_0$	1.044	1.108	1.32
$m_1$	4.173	4.245	4.120
$m_2$	0.530	0.526	0.504
$m_3$	11.157	10.942	10.304

## 2.2. The photosynthesis model and its parameterization

The daily rates of the carbon fixation ( $PP$  or  $P$ ; in units of  $\text{mgC.m}^{-2}.\text{d}^{-1}$ ) by phytoplanktonic cells was estimated using a classical photosynthesis versus light ( $P$  vs  $E$ ) model:

$$P = chl \cdot P_{\max}^B \cdot \int_{t=0}^{24h} \int_{z=0}^{0.1\%} \left( 1 - \exp \left[ \frac{-PUR(z,t)}{E_k(z)} \right] \right) dt dz, \quad (5)$$

where  $chl$  is the chlorophyll-a concentration in  $\text{mg Chl-a m}^{-3}$ ,  $P_{\max}^B$  is the light-saturated Chl-a-normalized carbon fixation rate in  $\text{mg C} (\text{mg Chl-a})^{-1} \cdot \text{h}^{-1}$ ,  $E_k(z)$  is the saturation irradiance in moles quanta  $\text{m}^{-2} \cdot \text{s}^{-1}$  and  $PUR(z,t)$  is the Photosynthetically Usable Radiation expressed in mole quanta  $\text{m}^{-2} \cdot \text{s}^{-1}$  (sensus Morel 1978). PUR is the Photosynthetically Active Radiation (PAR) weighted by the  $chl$ -specific phytoplankton absorption spectrum  $a_{phyto}(\lambda)$  :

$$PUR(z,t) = \int_{\lambda=400}^{700} \frac{a_{phyto}(\lambda)}{a_{phyto}(443)} E^0(\lambda, z, t) d\lambda, \quad (6)$$

where  $E^0(\lambda, z, t)$  is the spectral scalar irradiance at depth  $z$  and time  $t$ . The scalar irradiance was obtained using an approximation of the RTE (Morel 1991):

$$E^0(\lambda, z, t) = E_d(\lambda, z, t) \cdot \frac{K_d(\lambda)}{a(\lambda)} \quad (7)$$

where  $K_d(\lambda)$  is given by eq. 4 and  $a(\lambda)$  from the OC observations using the QAA algorithm (see the previous section). The *chl*-specific phytoplankton absorption coefficient was obtained from the statistical relationship between chl and  $a_{phyto}(\lambda)$  established by Matsuoka et al (2007) from data collected in the Arctic Ocean (Fig. 2). Note that only the spectral shape of  $a_{phyto}(\lambda)$  was considered in the current study in the estimation of PUR (eq. 6).

Two photosynthetic parameters,  $P_{max}^B$  and  $E_k$ , are needed in eq 5. The latter parameter varies as a function of the light environment following the model established by Arrigo and Sullivan (1994):

$$E_k(z) = \frac{E_k^{\max}}{1 + 10 \exp[-B \cdot PUR(z)]}, \quad (8)$$

$$B = \exp[1.089 - 2.12 \cdot \log(E_k^{\max})], \quad (9)$$

where  $E_k^{\max}$  is the maximum  $E_k$  value observed and was taken as 80 moles quanta.m<sup>-2</sup>.s<sup>-1</sup> as observed in Antarctica by Arrigo et al., (1998), Fig. 2. The Arctic phytoplankton was thus assumed to have the same adaption to light as the Antarctic phytoplankton.  $\overline{PUR(z)}$  is the mean daily PUR at depth z, and is obtained as follows :

$$\overline{PUR(z)} = \frac{\int_{t=0}^{24h} PUR(z, t) dt}{DayLength}, \quad (10)$$

where DayLength is the day length in seconds (photoperiod).

The last parameter,  $P_{max}^B$ , was assumed to have a constant value of 2.0 mg C (mg CHL)<sup>-1</sup> h<sup>-1</sup>, an average value based on field measurements in Arctic waters (Harrison and Platt, 1986; Sakshaug and Slagstad, 1991).

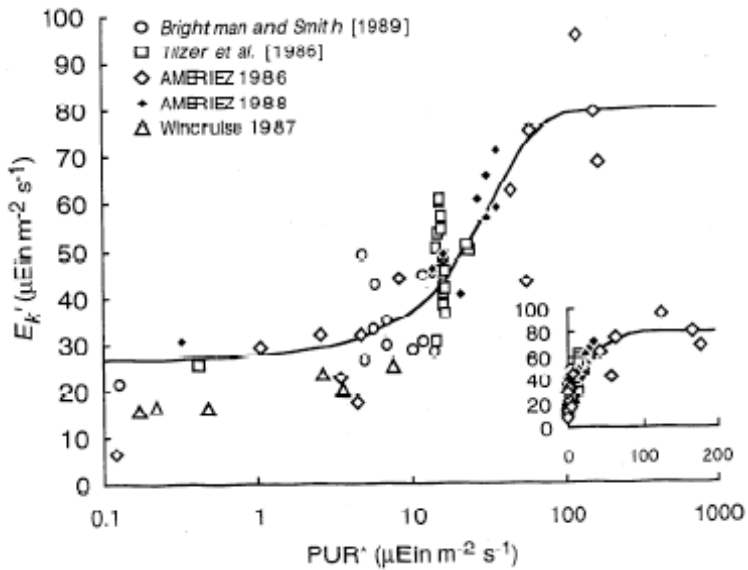


Figure 2 – Variation of the saturation irradiance parameter as a function of the mean daily PUR (reproduced from Arrigo et al. 1998).

### 2.3 Computation specifications

The spatial and time resolutions of the computation were determined by those of the data input into the model (Table 2 and section 3). The current PP model was designed to produce an estimation of PP at every pixel where OC data are available. The procedure used for the ingestion of satellite imagery follows the logic presented in figures 3 and 4.

For each ocean pixel, a check is made to determine if OC data of the current month is available. If no data is available for that month, then it is checked whether the pixel had been previously documented during the 13 years of OC observations, i.e. in the monthly climatology. If OC data is available, the daily PP is computed for each day of the month. The final daily production rate of the pixel is adjusted as a function of the fraction of open water pixels, (1-SIC) where SIC is the sea ice concentration (see section 3.3). Note that PP is computed only if open water area is greater than 5%, which happens frequently near the central ice pack when using OC climatology values. Spectral irradiance is computed every 3-hours using the EdLUT with ISCCP data input spatially interpolated to the OC pixel position, i.e. from the ISCCP 280-km grid to the OC Integerized Sinusoidal (ISIN) grid of 4.63 or 9.28-km resolution.

This scheme contrasts drastically from the PP models that are found in the literature. Most of these models deal with the global ocean where gaps in the OC coverage may not be significant. In the Arctic, the lack of OC data can significantly bias the total production estimates due to the persistent cloud cover and the presence of sea ice (See section 4).

Table 2 – Time and spatial resolution of the data input to the PP model.

Input data	Time resolution	Spatial resolution
Atmospheric parameters: $O_3$ , CF, $\tau_{cl}$	3-h	280-km
Sea ice concentration	Daily	25-km
Ocean color: $R_{rs}(\lambda)$ and chl	Monthly	9.28-km (NASA/MEaSUREs) 4.63-km (Globcolour)

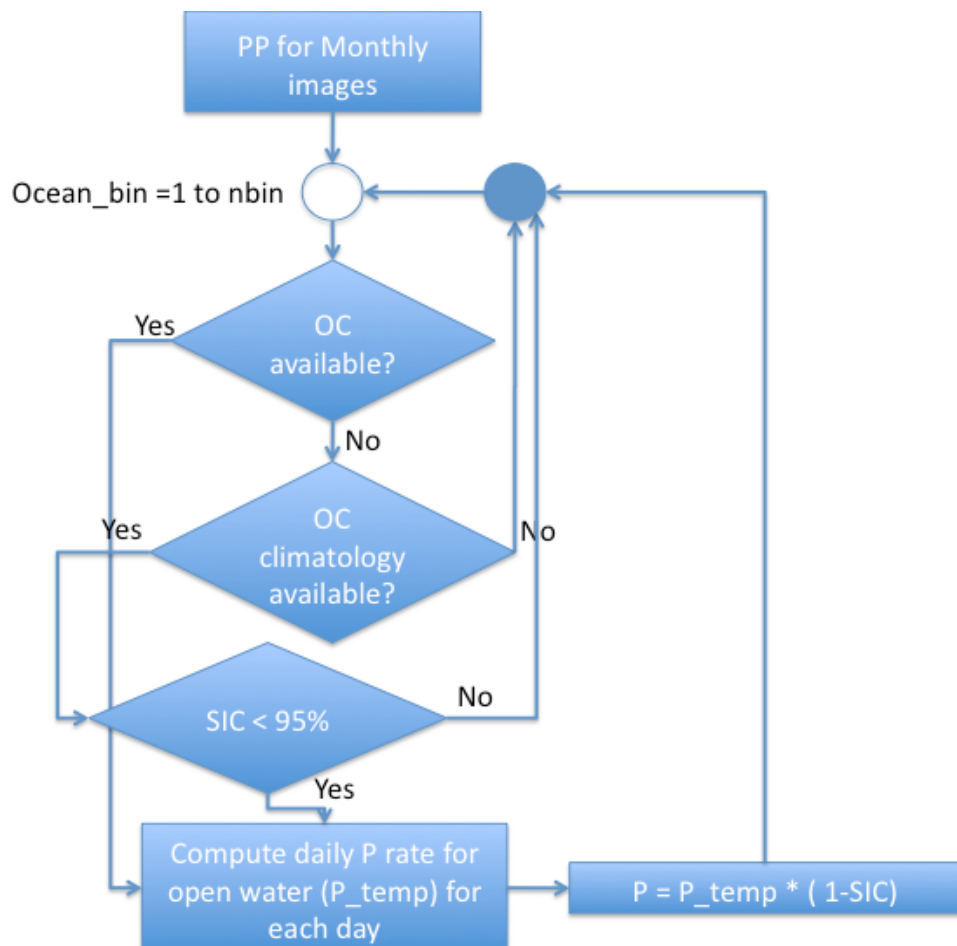


Figure 3 – Decision scheme of the PP model when processing a monthly image (see text for details).

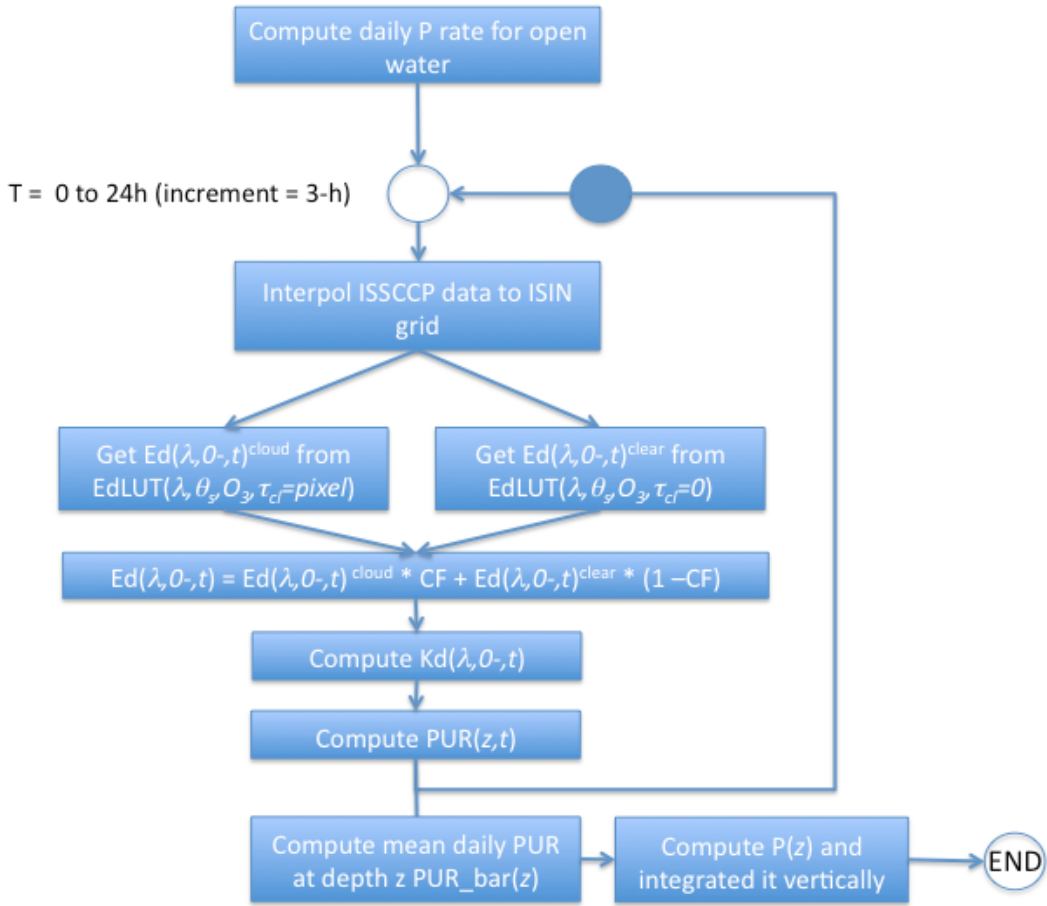


Figure 4 –Algorithm flowchart showing the daily PP rate computations for an ocean pixel (open water). See text for details.

In summary, PP is calculated for a monthly image at the spatial resolution of the OC data (4.63 or 9.28-km, Figure 3). For each day of the month, the daily PP rate is computed in steps of 3-hours (Figure 4). The daily PP rate for open water is then estimated by taking into account the open water area given by the daily sea ice data (Figure 3).

### 3. Model's inputs

#### 3.1. Ocean Color data

Monthly fully-normalized spectral water-leaving radiances (Globcolour;  $L_{wn}$ ) or reflectance (NASA;  $R_{rs}$ ) at 412, 443, 490, 510, 555 and 670 nm, as well as chl (Globcolour or MEaSUREs) were downloaded either from the ESA Globcolour project (<http://www.globcolour.info/>), the NASA GSFC (<http://oceandata.sci.gsfc.nasa.gov/>), or the MEaSUREs project

(<http://wiki.icesc.ucsb.edu/measures/index.php/GSM>) websites. Monthly-binned data from Globcolour are available at a 4.63 km resolution on an equal-area Integized Sinusoidal grid (ISIN). The NASA/MEaSUREs images that are provided at the 9.28-km resolution are also on an ISIN grid (see Globcolour PUG and the related NASA technical documentation in the bibliography section).  $L_{wn}$  or  $R_{rs}$  were used to retrieve the IOPs ( $a$  and  $b_b$ ) using the QAA at the SeaWiFS wavebands. Both Globcolour and MEaSUREs projects distribute the *chl* computed using a semi-analytical ocean IOPs retrieval algorithm developed by Garver and Siegel (1997) and optimized for *chl* estimations for SeaWiFS by Maritorena et al (2001) (hereinafter called GSM01). GSM01 implicitly accounts for Colored Detrital Material absorption (CDM = CDOM + NAP), which is important parameter in coastal arctic waters (Bélanger et al. 2008). CDM and suspended sediments affect less the *chl* retrieval with GSM01 than they do with the standard empirical algorithms (Ben Mustapha et al., submitted manuscript to *Remote Sensing of Environment*).

An example of the monthly *chl* maps of June 1998, as observed by SeaWiFS, is shown in Fig. 5a. Black pixels are areas where no SeaWiFS data is available due to the persistent presence of clouds (e.g. in the Bering Sea) or sea ice (e.g. Chuckchi, Laptev and Barents seas, and around the sea ice cover) during the whole month of June 1998. Figure 5b is the *chl* climatology for the month of June computed using the 13 years of SeaWiFS observations. The climatology was used to fill in the gaps in the observed data (Fig. 5c), resulting in a more complete image of the chlorophyll a field (see also Fig. 3).

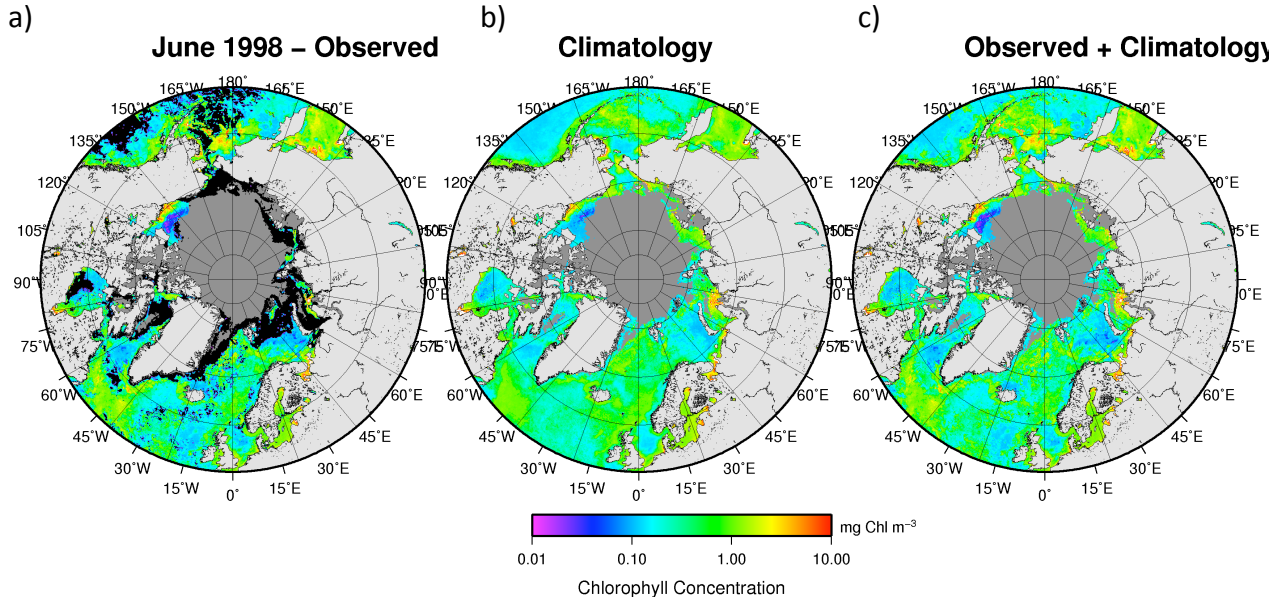


Figure 5 - Example of a monthly *chl* map, retrieved by applying the GSM01 algorithm on SeaWiFS data of June 1998. Gaps in the data were filled in with climatological data that was computed over 13-years (median method, see section 4.2 for details).

### 3.2 Atmospheric data

The atmospheric parameters that are necessary to estimate the incident irradiance were obtained from the International Satellite Cloud Climatology Project (ISCCP). ISCCP collects and analyzes satellite radiance measurements to infer the global distribution of clouds and their diurnal, seasonal, and interannual variations. Cloud optical thickness and cloud fraction retrieved following the approach by Zhang et al. (2004) were obtained from the surface radiative flux (SRF) data set (<http://isccp.giss.nasa.gov/products/products.html>). The SRF data set also includes satellite-derived total ozone column observations of the Total Ozone Mapping Spectrometer (TOMS). Global maps are distributed on a 280-km resolution equal-area grid at every 3-hours from 1983 to 2007. Similarly, a climatology was computed for the 1998 to 2007 period and was used in the PP processing for 2008, 2009 and 2010. An example of the SRF products is shown on figure 6.

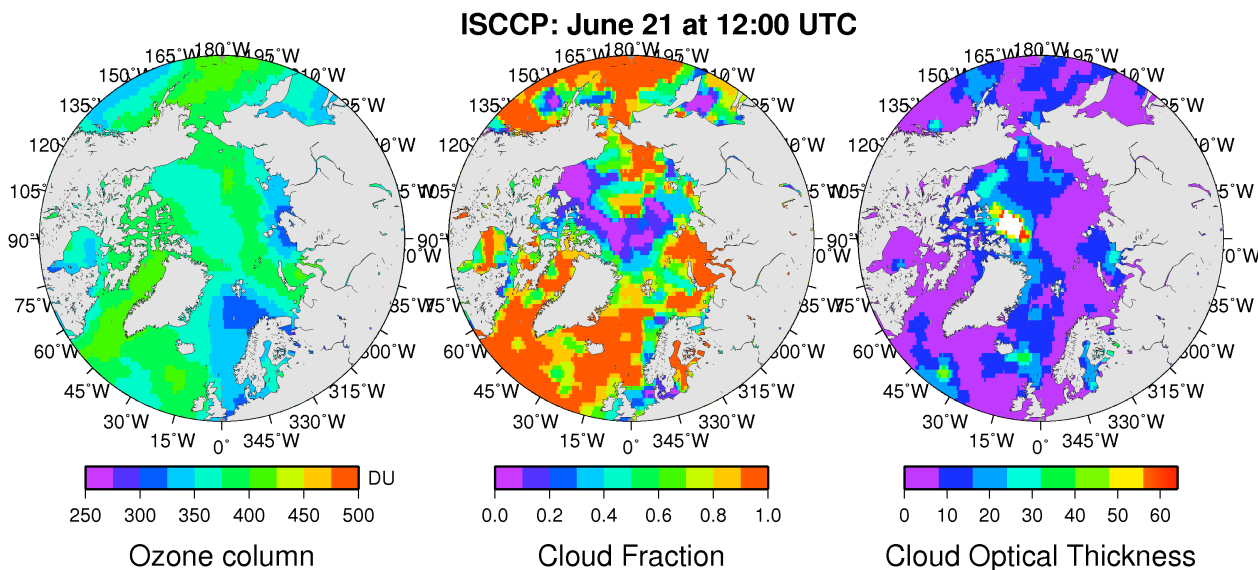


Figure 6 - Example of ISCCP SRF atmospheric products that are used as inputs into the  $E_d(\lambda, 0, t)$  LUT for the 21<sup>st</sup> of June 1998 at 12:00 UTC. The cloud fraction and cloud optical thickness were determined following the method of Zhang et al (2004), while O<sub>3</sub> is from TOMS observations.

### 3.3 Sea ice data

Satellite-derived sea ice concentration (SIC) was obtained from the National Snow and Ice Data Center (NSIDC). SIC are retrieved from passive microwave data of the SSMI (1998-2006) and AMSR-E sensors (2007 to present) using the NASA team algorithm (Cavallieri et

al., 1992; Comiso et al., 2003). Daily SIC pixels are distributed over a polar stereographic grid of 25-km resolution. An example of SIC for the 21<sup>st</sup> of June 21 is shown in figure 7. Note how open waters matches the SeaWiFS data availability (Fig. 5a), except for the Bering Sea where the lack of SeaWiFS data was due to a persistent cloud cover.

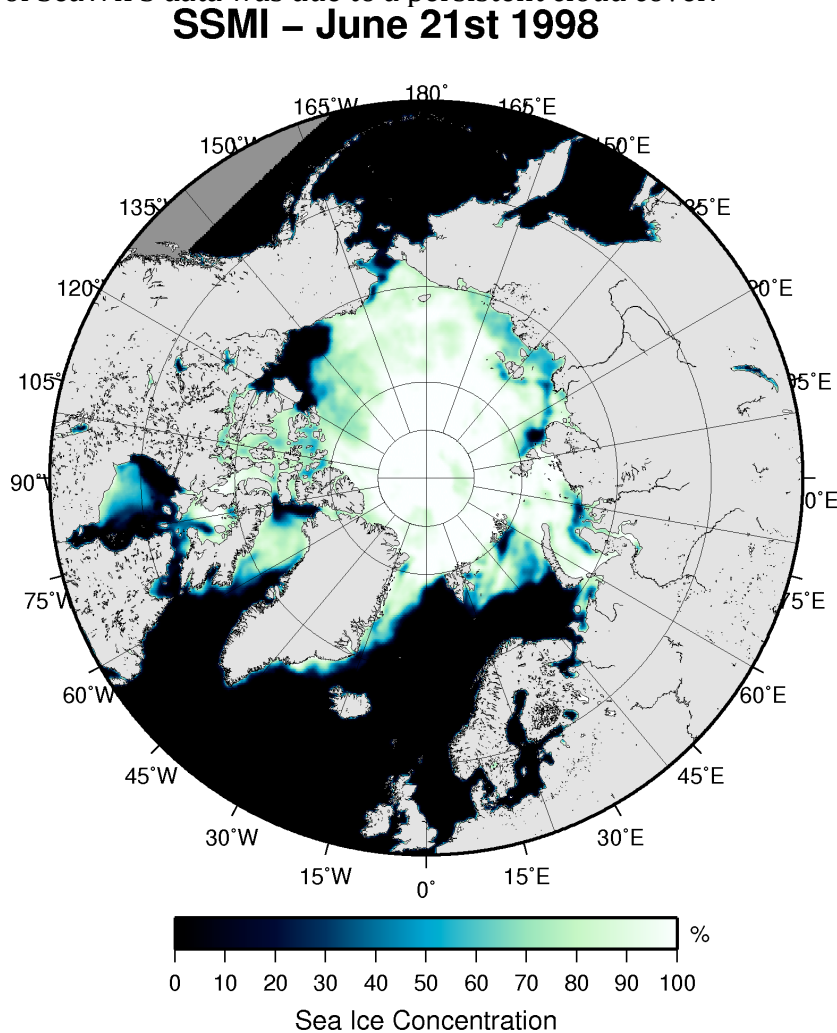


Figure 7 – Example of 25-km resolution sea ice concentration derived from the SSMI image of June 21<sup>st</sup>, 1998.

## 4. Sensitivity Analysis

A number of sensitivity tests were performed to assess the impact of the choices made for the PP model. First, the impact of the OC data availability on the yearly PP estimates needed to be assessed because OC measurements cannot be observed through clouds and when sea ice is

nearby. It was hypothesized that ignoring open waters under cloud cover and in the vicinity of sea ice can lead to a severe underestimation of PP. Second, we rely on a monthly climatology to fill in the gaps in OC observations in order to minimize the problem of OC data availability. It was found, however, that the method used in the generation of the climatology has a significant impact on the magnitude of the PP estimation. This is related with the non-normality of the ocean data frequency distribution (see next section).

#### 4.1. Impact of Ocean Color data availability

The number of pixels documented by SeaWiFS for each individual year of observation is shown in figure 8 (green line), which is, as expected, 15 to 20% less than the number of pixels found in the climatology. This is mainly due to the interannual variations and the displacement of the central arctic pack ice, which moves around the Arctic Ocean. SeaWiFS documented as much as 20000 more pixels in 2007 as compared to 1998. This represents an area of about 1.7 million km<sup>2</sup> (~ the area of Alaska). The number of documented pixels drops in 2008 and 2009 due to the frequent failure of the SeaWiFS sensor. Indeed no SeaWiFS data were available for January, February, March and July 2008, and January, May, September, October and November 2009.

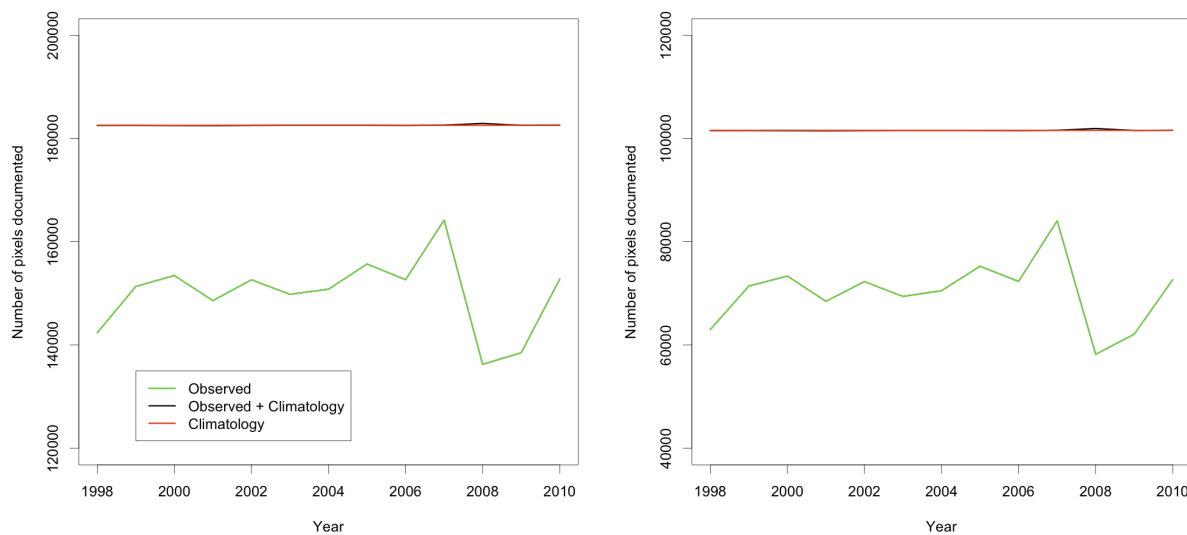


Figure 8 – Time-series of the number of pixels documented by SeaWiFS used to estimate the yearly PP for the Arctic Ocean and sub-arctic seas (left panel) and the circumpolar Arctic ( $>66.58^{\circ}\text{N}$ ; right panel).

An example of the monthly maps of PP for June 1998 is shown in figure 9. Pixels that were not documented due to the presence of sea ice show low PP rates ( $<1 \text{ gC month}^{-1}$ ; e.g. the Russian continental shelves, the central Baffin Bay), while areas not available due to persistent cloud cover show PP rates similar to their surrounding pixels ( $\sim 1 \text{ to } 10 \text{ gC month}^{-1}$ ; e.g. North Pacific; Bering Sea). The total primary production in June 1998 for the

Arctic Ocean and its surrounding seas reaches 93.4 and 119.6 TgC for the available OC pixels only and with the gaps in OC data replaced by the climatology, respectively. The impact of missing pixels represents, therefore, a missing PP of nearly 25%.

A similar underestimation was observed for the yearly PP calculated over the 13 years of SeaWiFS measurements (Figure 10). The underestimation for the circumpolar Arctic (i.e. latitude  $> 66.58^{\circ}\text{N}$ ) was, on the average, 39% (Table 3). Interestingly, considering all documented pixels does not significantly affect the actual trend in PP observed during the SeaWiFS era (Table 3). More importantly, the relative increase in PP is less pronounced when considering all pixels. For example, Arrigo et al. (2008) reported that the annual production of 2007 was 23% higher than the average production for the 1998-2002 period. Our results rather indicate an increase of 28% in 2007 relative to the 1998-2002 period when only available pixels were considered in the PP calculation. Interestingly that number drops to 14% when considering all pixels, making the change in PP less dramatic than suggested by Arrigo et al (2008)'s results.

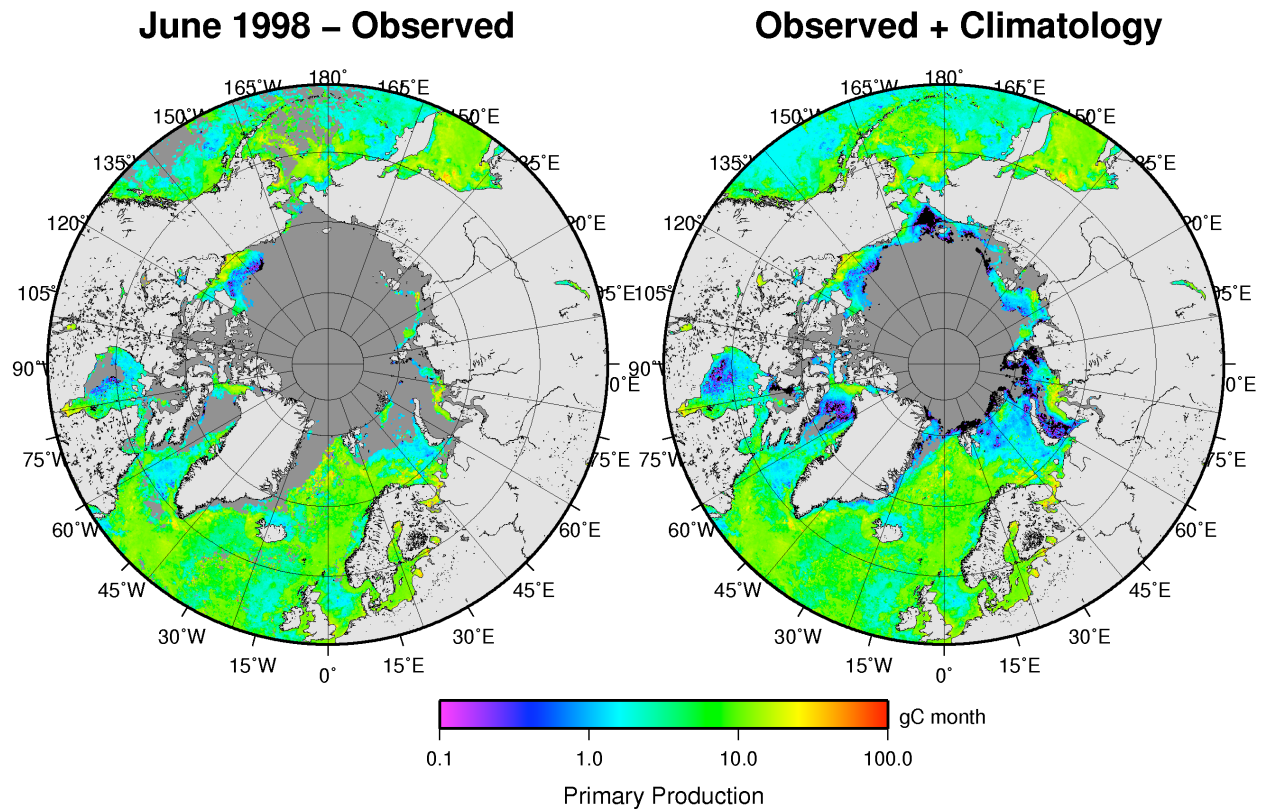


Figure 9 – Monthly maps of PP in June 1998. The production rates are calculated only for available OC pixels (left panel) and with the gaps in OC data replaced by the climatology.

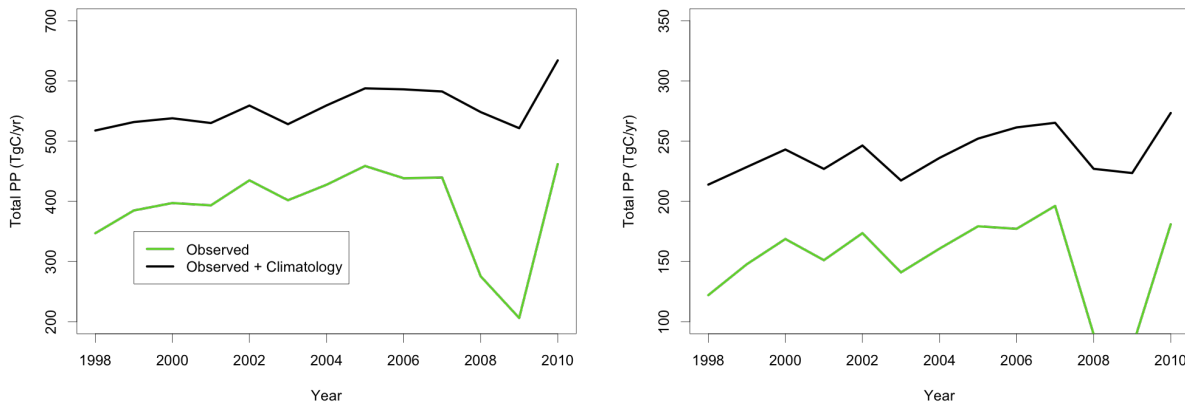


Figure 10 - Time-series of the total annual PP for the Arctic Ocean and sub-arctic seas (left panel) and the circumpolar Arctic (right panel) using only SeaWiFS observations (green lines) and when the gaps in the OC data were replaced by the climatological values (black lines).

Table 3 – Impact of OC data availability on the yearly PP and the trends

Ocean color data input	Arctic Ocean and sub-arctic seas		Circumpolar Arctic	
	Mean PP <sup>1</sup> (Tg yr <sup>-1</sup> )	Trends <sup>3</sup> (Tg decade <sup>-1</sup> ) (r <sup>2</sup> )	Mean PP <sup>1</sup> (Tg yr <sup>-1</sup> )	Trends (Tg decade <sup>-1</sup> ) (r <sup>2</sup> )
Only Observed pixels	416.8	84.5 (0.78)	163.5	44.2 (0.57)
Observed, but with gaps replaced by climatology data	559.5	89.4 (0.86)	242.2	45.0 (0.70)
<b>Relative difference<sup>2</sup></b>	29%	6%	39%	<1%

<sup>1</sup> Statistics and trends calculation exclude 2008 and 2009.

<sup>2</sup> Relative difference = (observed\_clim - observed)/mean(observed\_clim , observed)

<sup>3</sup> The trend is the slope of a linear regression between time and yearly PP.

## 4.2. Impact of the method used to calculate the climatology

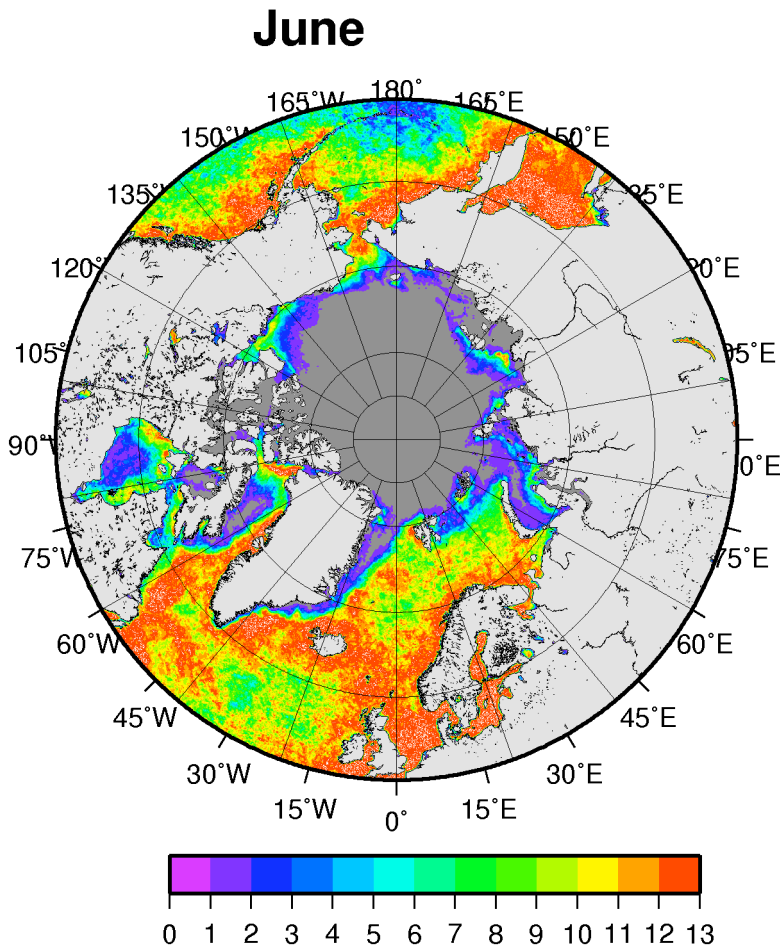
SeaWiFS Level 3 data are temporally and spatially averaged using the level 2 observations that have a nominal resolution of 1.1 km. The L3 data are binned onto an equal area grid of 9.28 km resolution for different time periods (for 1-day, 8-days, month, etc.). The averaging method adopted by NASA consists of a simple arithmetic average and gives the same weight to every pixel. This method was adopted by NASA despite the fact that OC measurements such as *chl* tend to be lognormally distributed, i.e.  $\log(chl)$  is normally distributed in large satellite data sets (Campbell et al., 1995). The reason for that choice over the method that was initially proposed by Campbell et al. (1995), i.e. a maximum likelihood estimator based on log-transformed data (MLE), was motivated by the unstable behavior of the MLE ([http://oceancolor.gsfc.nasa.gov/forum/oceancolor/topic\\_show.pl?pid=98;hl=method%20binning#pid98](http://oceancolor.gsfc.nasa.gov/forum/oceancolor/topic_show.pl?pid=98;hl=method%20binning#pid98))

Because many pixels are missing at latitudes greater than 50°N due to clouds and sea ice, it was necessary to apply a method to fill in the gaps in the monthly data in order to obtain a consistent data set for the subsequent time-series analysis. Here we adopted the methodology of filling in the gap in a given monthly image by the value found in the climatology when available. Note that a more robust method exists but is not applicable at high latitudes because too many gaps are present in the dataset due to clouds, low solar zenith angles and sea ice (Yoder and Kennelly, 2003).

It was found that the method that is being employed during the generation of the monthly OC climatology is of a great importance. Tested methods are:

- i. IOPs and *chl* retrieved from the monthly  $L_{wn}(\lambda)$  climatologies provided by the space agencies (NASA and ESA) (hereinafter CLIM\_LWN);
- ii. Monthly IOPs and *chl* averaged using an arithmetic mean (e.g. 13 months of June from 1998 to 2010 averaged to obtain the June climatology) (CLIM\_AVG);
- iii. Monthly IOPs and *chl* averaged using a geometric mean, i.e. a mean on log-transformed data (CLIM\_GEO);
- iv. The median of the monthly IOPs and *chl* observations (CLIM\_MEDIAN).

Figure 11 presents the number of pixel used to generate the June climatology with the CLIM\_AVG, CLIM\_GEO and CLIM\_MEDIAN methods. In permanently open waters (North polar Atlantic and Pacific; Nordic seas), the number of documented pixels is generally greater than 9, except in regions close to the atmospheric polar front located between 50 and 60°N. This number drops near the seasonal sea ice area. Note the few exceptions found in regions known as polynyas such as the North Water, the cap Bathurst, the northern Hudson Bay and the southern Laptev sea, where the number of observations is relatively more important than their surroundings.



Number of pixels used to generate the Climatology

Figure 11 – Map of the number of pixels used to generate the climatology following the CLIM\_AVG, CLIM\_GEO and CLIM\_MEDIAN methods (see text).

Table 4 presents the average yearly PP for the SeaWiFS era calculated using the four climatologies of the IOPs and *chl* that were used in filling in the gaps. As a comparison, yearly PP was also calculated by forcing the model to use the climatology for every year from 1998 to 2010. When the yearly PP calculated by forcing the climatology is higher than that obtained using the observation with filled gaps, this means that averaging method used to calculate the climatology tends to give more weight to high values of *chl*. This is the case for CLIM\_LWN and CLIM\_AVG. In contrast, when the climatology gives a lower PP estimate than the one obtained using the observation with filled gaps, this means that the averaging method tends to give more weight to low *chl* values. This is the case for CLIM\_GEO and CLIM\_MEDIAN. For the circumpolar Arctic, there is as much as 35% difference between the yearly PP calculated when forcing the model to use the climatologies following the CLIM\_GEO and CLIM\_LWN methods. When climatology is only used to fill in the gaps in the

observation, the effect is less important but still somewhere between CLIM\_GEO and CLIM\_LWN ( $\sim 10\%$ ).

The choice of the climatology computation method on the time-series trends is less important than it is for the absolute PP estimation (Table 5). Because the number of pixels taken in the climatology tends to increase with time (Fig. 8), the methods giving more weight to high *chl* values (CLIM\_LWN and CLIM\_AVG) result in a lower increase in PP over time (i.e. the trend) than the methods giving more weight to low *chl* values (CLIM\_GEO and CLIM\_MEDIAN). Nevertheless, the largest difference between the four methods is smaller than 8%.

Based on these results, the climatology that was built using the median was chosen because the gaps in the observation are replaced by a conservative concentration of *chl*.

Table 4 – Yearly PP estimates using various methods to compute the monthly climatology (SeaWiFS)

Method	Observed, with gaps filled with climatology		Climatology	
	Arctic and sub-arctic seas (TgC y $^{-1}$ )	Circumpolar Arctic (>66.58°N) (TgC y $^{-1}$ )	Arctic and sub-arctic seas (TgC y $^{-1}$ )	Circumpolar Arctic (>66.58°N) (TgC y $^{-1}$ )
CLIM_LWN	593	258	657	285
CLIM_AVG	587	255	639	270
CLIM_GEO	546	234	493	207
CLIM_MEDIAN	556	240	516	218
Average (SD)	570.5 (23)	246.75 (11.6)	576.25 (83.7)	245 (38.3)

Table 5 – Decadal trends in PP obtained using various methods to compute the monthly climatology (SeaWiFS)<sup>1</sup>

Method	Observed, with gaps filled with climatology		
	Arctic and sub-arctic seas (TgC decade $^{-1}$ )	Circumpolar Arctic (>66.58°N) (TgC decade $^{-1}$ )	Circumpolar Arctic (>66.58°N) (TgC decade $^{-1}$ )
CLIM_LWN	86.1	41.9	41.9
CLIM_AVG	87.6	42.7	42.7
CLIM_GEO	90.3	45.4	45.4
CLIM_MEDIAN	89.4	45.0	45.0

<sup>1</sup> Trends are obtained applying a linear fit between yearly PP and time, excluding 2008 and 2009 due to frequent sensor failure that happened during those years.

## 5. Known limitations of the methodology

Table 6 presents a summary of the known potential sources of bias of the methodology. It gives the order of importance based on our current knowledge of the performance of the algorithm. When possible, it also indicates what to expect in terms of absolute estimations of PP, whether it would cause an overestimation or an underestimation. Most of these issues, if not all, require more research and validation using *in situ* observations.

Table 6 – Known limitations of the PP model or the data input accuracy.

Issue	Description	Order of importance	Expected impact on PP
<b>1) Downwelling irradiance <math>E_d(\lambda)</math></b>			
a) surface reflectance assumption	EdLUT was constructed assuming an ocean surface without sea ice. The presence of sea ice creates multiple scattering between ice and the lower atmosphere. This phenomenon increases the number of photons per m <sup>2</sup> that would enter open waters located nearby.	2 <sup>nd</sup>	Increase
b) atmospheric aerosol assumption	EdLUT was constructed assuming a constant value of marine aerosol optical thickness (AOT) of 0.1, which is an average at the global scale. Average AOT at Point Barrow, Alaska, is rather around 0.06. In contrast, the arctic's atmosphere is known as to be contaminated by man-derived aerosols causing the arctic haze.	2 <sup>nd</sup>	Unknown
<b>2) Ocean color data</b>			
a) $L_{wn}$ retrieval	Several potential problems may affect the quality of the $L_{wn}$ retrieval. Sea ice is known to contaminate OC retrievals (Bélanger et al 2007). Current L3 binning methods do not eliminate pixels contaminated by sea ice despite the fact that new methods have been proposed (Bélanger et al 2007; Wang and Shi 2009). Besides, atmospheric correction schemes may be problematic due 1) to low signal-to-noise when solar elevation is low, 2) to the unknown effect of earth's curvature; 3) to water turbidity in the coastal waters affected by the runoff by rivers and coastal erosion. Those problems may severely affect the quality of the retrieval at the 412 nm spectral channel, which is used in our approach.	1 <sup>st</sup>	Unknown

Table 6 - Continued

Issue	Description	Order of importance	Expected impact on PP
b) IOPs ( $a, b_b$ ) retrieval	The IOP retrieval relies heavily on the quality of the water-leaving radiance measurements from space. Even if $L_{wn}$ had been retrieved without error, its inversion to estimate IOPs is not perfect. The QAA was chosen for its simplicity and its good performance in providing total $a, b_b$ as compared with the other inversion methods (IOCCG, 2006). Preliminary validation of the QAA in the Arctic waters suggests that it underestimates $a$ at short wavelengths (412, 443) in the Beaufort Sea coastal waters (Bélanger 2006).	2 <sup>nd</sup>	unknown
c) <i>chl</i> retrieval	<i>Chl</i> is retrieved using a semi-analytical model, GSM01, optimized for the open ocean, non-polar waters (Maritorena et al 2002). A residual effect of CDM is expected since the spectral shape of CDM in the arctic may differ from that of the global ocean. Similarly, polar phytoplankton is subject to the pigments' packaging effect that depresses its specific-absorption spectra. The overall effect of this feature on the <i>chl</i> retrieval is unknown. Contradicting validation results have been obtained so far (Wang and Cota 2003; Ben Mustapha et al, submitted)	1 <sup>st</sup>	unknown
<b>3) Sea ice concentration</b>	Sea ice concentration (SIC) was derived from passive microwave sensed from space. Recent investigations suggest that SIC is underestimated during the summer months due to confounding effect of melt ponds at sea ice surface. The underestimation may be especially important during the summer season where the PP is at its maximum.	2 <sup>nd</sup>	Decrease
<b>4) PP model assumptions</b>			
a) <i>chl</i> and IOPs vertical structure	The model assumes a vertical homogeneity of the IOPs and the biomass of the water column. A recent study clearly indicates the near-ubiquity of the sub-surface chlorophyll-a maximum (SCM) (Martin et al 2010). The Arctic SCM tends to be located between 3 to 10% of light levels, which markedly contrast with the global ocean SCM that usually is <1% light level (Uitz et al., 2006). Consequently, SCM accounts for a significant proportion of the PP (Martin et al., 2010). The vertical homogeneity assumption may be the most important bias of our approach. Alternative methods to model the <i>chl</i> profiles is urgently needed	1 <sup>st</sup>	Increase

(e.g. Morel and Berthon 1989).

---

Table 6 - Continued

Issue	Description	Order of importance	Expected impact on PP
b) The light-saturated <i>chl</i> -normalized carbon fixation rate $P_{\max}^B$ .	$P_{\max}^B$ is often known to vary as a function of temperature or light history of phytoplankton (Behrenfeld et al 2002). The variability of this parameter in the Arctic is still not well known. In addition, most data comes from late summer. Very few data during the spring bloom are available.	1 <sup>st</sup>	Unknown
<b>5) Numerical issues</b> a) Time step of OC data	Monthly OC data may introduced some bias due to the binning method employed to generate the L3 data (see section 4.2). To avoid introducing any bias due to the L3 binning processes, PP would need to be calculated using daily OC observations with the gaps filled in using temporal interpolation between available data before and after that day. Such calculation would require more computation time.	2 <sup>nd</sup>	Unknown

---

## 6. Conclusions

We have presented the theoretical basis of a PP model design for the Arctic waters. The most important advantage of this model relative to other approach is the consideration of the propagation of spectral light in the atmosphere and the ocean using methods appropriate for both case 1 and case 2 waters. The model's sensitivity can also be easily assessed by changing the model parameters (e.g. photosynthetic parameters), which are measurable on the field. Here we presented preliminary results of such sensitivity study. Model parameterization will be improved in the future when more in situ data become available.

Comparison with published PP estimates of Pabi et al. (2008) and Arrigo et al. (2008) indicates that our model yields total production value ~2-fold lower than their estimations. This is mostly due to the *chl* input, which is systematically higher when it is estimated using standard empirical algorithms (Ben Mustapha et al., submitted). Clearly, further work is needed to validate the model with in situ observation.

## 7. Bibliography

- Antoine, D., A. Morel, and J. M. André (1996), Oceanic primary production : II. Estimation at global scale from satellite (Coastal Zone Color Scanner) chlorophyll, *Global Biogeochem. Cycles*, 10(1), 57-69.
- Arrigo, K. R., D. Worthen, A. Schnell, and M. P. Lizotte (1998), Primary production in Southern Ocean waters, *J. Geophys. Res.*, 103(C8), 15587-15600.
- Arrigo, K. R., G. van Dijken, and S. Pabi (2008), Impact of a shrinking Arctic ice cover on marine primary production, *Geophys. Res. Lett.*, 35(19), L19603.
- Arrigo, K. R., and C. W. Sullivan (1994), A high resolution bio-optical model of microalgal growth: Tests using sea-ice algal community time-series data, *Limnol. Oceanogr.*, 39(3), 609-631.
- Behrenfeld, M. J., and P. G. Falkowski (1997), Photosynthetic rates derived from satellite-based chlorophyll concentration, *Limnol. Oceanogr.*, 42(1), 1-20.
- Behrenfeld, M. J., E. Boss, D. A. Siegel, and D. S. Shea (2005), Carbon-based ocean productivity and phytoplankton physiology from space, *Global Biogeochem. Cycles*, 19, GB1006.
- Behrenfeld, M. J., E. Marañón, D. A. Siegel, and S. B. Hooker (2002), Photoacclimation and nutrient-based model of light-saturated photosynthesis for quantifying oceanic primary production, *Mar. Ecol. Progr. Series*, 228, 103-117.
- Bélanger, S. (2006), Response of light-related carbon fluxes in the Arctic Ocean to climate change: quantification and monitoring of dissolved organic matter photo-oxidation in the Beaufort Sea using satellite remote sensing, *Ph.D.*, 243.
- Bélanger, S., M. Babin, and P. Larouche (2008), An empirical ocean color algorithm for estimating the contribution of chromophoric dissolved organic matter to total light absorption in optically complex waters, *J. Geophys. Res.*, 113(C4), 1-14, doi:10.1029/2007JC004436.
- Bélanger, S., J. Ehn, and M. Babin (2007), Impact of sea ice on the retrieval of water-leaving reflectance, chlorophyll a concentration and inherent optical properties from satellite ocean color data, *Remote Sens. Environ.*, 111(1), 51-68, doi:10.1016/j.rse.2007.03.013.
- Campbell, J. W., J. M. Blaisdell, and M. Darzi (1995), Level -3 SeaWiFS Data Products : Spatial and Temporal Binning Algorithms, in *Nasa Technical Memorandum, Volume 32*, vol. 32, edited by S. B. Hooker, E. R. Firestone, and J. G. Acker, p. 80 pp., Greenbelt, MD.
- Campbell, J. et al. (2002), Comparison of algorithms for estimating ocean primary production from surface chlorophyll, temperature, and irradiance, *Global Biogeochem. Cycles*, 16(3), 1035.
- Carr, M.-E. et al. (2006), A comparison of global estimates of marine primary production from ocean color, *Deep Sea Res. Part II*, 53(5-7), 741-770.
- Cavalieri, D. J. (1992), *Cavalieri, D. J., ed., 1992. NASA Sea Ice Validation Program for the Defense Meteorological Satellite Program Special Sensor Microwave Imager: Final Report*, Washington, D.C.
- Comiso, J.C., Cavalieri, D.J., Markus, T. (2003), Sea ice concentration, ice temperature, and Arctic PP model ATBD

- snow depth using AMSR-E data, *IEEE Transactions on Geoscience and Remote Sensing*, 41(2), 243 – 252.
- Garver, S., and D. Siegel (1997), Inherent optical property inversion of ocean color spectra and its biogeochemical interpretation 1. Time series from the Sargasso Sea, *J. Geophys. Res.*, 102, 18607-18625.
- Globcolour, <http://www.globcolour.info>
- Globcolour, [http://www.globcolour.info/CDR\\_Docs/GlobCOLOUR\\_PUG.pdf](http://www.globcolour.info/CDR_Docs/GlobCOLOUR_PUG.pdf)
- Harrison, W. G., and T. Platt (1986), Photosynthesis-irradiance relationships in polar and temperate phytoplankton populations, *Polar Biology*, 5, 153-164.
- Lee, Z. P., M. Darecki, K. L. Carder, C. O. Davis, D. Stramski, and W. J. Rhea (2005), Diffuse attenuation coefficient of downwelling irradiance: An evaluation of remote sensing methods, *J. Geophys. Res.*, 110(C2), C02017.
- Lee, Z. P., K. P. Du, and R. Arnone (2005), A model for the diffuse attenuation coefficient of downwelling irradiance, *J. Geophys. Res.*, 110(C2), C02016.
- Lee, Z.-P., K. L. Carder, and R. A. Arnone (2002), Deriving inherent optical properties from water color : a multiband quasi-analytical algorithm for optically deep waters, *Applied Optics*, 41(27), 5755-5772.
- Maritorena, S., and D. Siegel (2005), Consistent merging of satellite ocean color data sets using a bio-optical model, *Remote Sens. Environ.*, 94, 429-440.
- Maritorena, S., D. A. Siegel, and A. R. Peterson (2002), Optimization of a semianalitical ocean color model for global-scale applications, *Applied Optics*, 41(15), 2705-2714.
- Martin, J., J. Tremblay, J. Gagnon, G. Tremblay, A. Lapoussière, C. Jose, M. Poulin, M. Gosselin, Y. Gratton, and C. Michel (2010), Prevalence, structure and properties of subsurface chlorophyll maxima in Canadian Arctic waters, *Mar. Ecol. Progr. Series*, 412, 69-84, doi:10.3354/meps08666.
- Matsuoka, A., Y. Huot, K. Shimada, S.-I. Saitoh, and M. Babin (2007), Bio-optical characteristics of the western Arctic Ocean: implications for ocean color algorithms, *Can. J. Remote Sensing*, 33(6), 503-518.
- McClatchey, R. A., R. W. Fenn, J. E. A. Selby, F. E. V. and J. S. G. (1971), *Optical properties of atmosphere*, Bedford, Massachusetts.
- Morel, A. (1978), Available, usable, and stored radiant energy in relation to marine photosynthesis, *Deep-Sea Res.*, 25, 673-688.
- Morel, A. (1988), Optical Modeling of the Upper Ocean in Relation to its biogenous matter content (Case 1 Waters), *J. Geophys. Res.*, 93(C9), 10749-10768.
- Morel, A. (1991), Light and marine photosynthesis: a spectral model with geochemical and climatological implications, *Progress in Oceanography*, 26, 263-306.
- Morel, A., and J.-F. Berthon (1989), Surface pigments, algal biomass profiles, and potential production of the euphotic layer: Relationships reinvestigated in view of remote-sensing applications, *Limnol. Oceanogr.*, 34(8), 1545-1562, doi:10.4319/lo.1989.34.8.1545.
- Morel, A., and S. Maritorena (2001), Bio-optical properties of oceanic waters: A reappraisal, *J. Geophys. Res.*, 106(C4), 7163-7180.
- NASA,[http://oceancolor.gsfc.nasa.gov/SeaWiFS/TECH\\_REPORTS/PreLPDF/PreLVol32.pdf](http://oceancolor.gsfc.nasa.gov/SeaWiFS/TECH_REPORTS/PreLPDF/PreLVol32.pdf)

- Pabi, S., G. L. van Dijken, and K. R. Arrigo (2008), Primary production in the Arctic Ocean, 1998–2006, *J. Geophys. Res.*, 113(C8), C08005. [online] Available from: <http://dx.doi.org/10.1029/2007JC004578> DOI - 10.1029/2007JC004578
- Perrette, M., A. Yool, G. D. Quartly, and E. E. Popova (2011), Near-ubiquity of ice-edge blooms in the Arctic, *Biogeosciences*, 8(2), 515-524, doi:10.5194/bg-8-515-2011.
- Platt, T., S. Sathyendranath, C. Caverhill, and M. R. Lewis (1988), Ocean primary production and available light: Further algorithms for remote sensing, *Deep-Sea Res.*, 35, 855-879.
- Ricchiazzi, P., S. R. Yang, C. Gautier, and D. Sowle (1998), SBDART: A research and teaching software tool for plane-parallel radiative transfer in the Earth's atmosphere, *B. Am. Meteorol. Soc.*, 79, 2101-2114.
- Sakshaug, E., and D. Slagstad (1991), Light and productivity of phytoplankton in polar marine ecosystems: a physiological view, *Polar Biology*, 10, 69-85.
- Sathyendranath, S., T. Platt, C. M. Caverhill, R. E. Warnock, and M. R. Lewis (1989), Remote sensing of oceanic primary production: computations using a spectral model, *Deep-Sea Res.*, 36(3), 431-453.
- Smyth, T. J., G. H. Tilstone, and S. B. Groom (2005), Integration of radiative transfer into satellite models of ocean primary production, *J. Geophys. Res.*, 110(C10), C10014.
- Uitz, J., H. Claustre, A. Morel, and S. B. Hooker (2006), Vertical distribution of phytoplankton communities in open ocean: An assessment based on surface chlorophyll, *J. Geophys. Res.*, 111, C08005, doi:10.1029/2005JC003207.
- Wang, J., and G. F. Cota (2003), Remote-sensing reflectance in the Beaufort and Chukchi seas: observations and models, *Applied Optics*, 42(15), 2754-2765.
- Wang, M., and W. Shi (2009), Detection of Ice and Mixed Ice-Water Pixels for MODIS Ocean Color Data Processing, *IEEE Transactions Geoscience and Remote Sensing*, 47(8), 2510-2518, doi:10.1109/TGRS.2009.2014365.
- Yoder, J. a, and M. A. Kennelly (2003), Seasonal and ENSO variability in global ocean phytoplankton chlorophyll derived from 4 years of SeaWiFS measurements, *Global Biogeochem. Cycles*, 17(4), 1112, doi:10.1029/2002GB001942.
- Zhang, Y. C., W. B. Rossow, A. A. Lacis, V. Oinas, and M. I. Mishchenko (2004), Calculation of radiative fluxes from the surface to top of atmosphere based on ISCCP and other global data sets: Refinements of the radiative transfer model and the input data, *J. Geophys. Res.*, 109, D19105.